ACS NANO
Cite This: ACS Nano 2019, 13, 3083−3094
www.acsnano.org

ARTICLE

In Situ Dendritic Cell Vaccine for Effective Cancer Immunotherapy

Weijing Yang,[†,‡] Guizhi Zhu,[‡] Sheng Wang,[‡] Guocan Yu,[‡] Zhen Yang,[‡] Lisen Lin,[‡] Zijian Zhou,[‡] Yijing Liu,[‡] Yunlu Dai,[‡] Fuwu Zhang,[‡] Zheyu Shen,[‡] Yuan Liu,[‡] Zhimei He,[‡] Joseph Lau,[‡] Gang Niu,[‡] Dale O. Kiesewetter,[‡] Shuo Hu,[*,†,§] and Xiaoyuan Chen[*,‡]

[†]Department of PET Center, Xiangya Hospital, Central South University, Changsha, 410008, China

[§]National Clinical Research Center for Geriatric Disorders (XIANGYA), Xiangya Hospital, Central South University, Changsha, 410008, China

[‡]Laboratory of Molecular Imaging and Nanomedicine (LOMIN), National Institute of Biomedical Imaging and Bioengineering (NIBIB), National Institutes of Health (NIH), Bethesda, Maryland 20892, United States

Supporting Information

ABSTRACT: **A cancer vaccine is an important form of immunotherapy. Given their effectiveness for antigen processing and presentation, dendritic cells (DCs) have been exploited in the development of a therapeutic vaccine. Herein, a versatile polymersomal nanoformulation that enables generation of tumor-associated antigens (TAAs) and simultaneously serves as adjuvant for an *in situ* DC vaccine is reported. The chimeric cross-linked polymersome (CCPS) is acquired from self-assembly of a triblock copolymer, polyethylene glycol-poly(methyl methyacrylate-*co*-2-amino ethyl methacrylate (thiol/amine))-poly 2-(dimethylamino)ethyl methacrylate (PEG-P(MMA-*co*-AEMA (SH/NH_2)-PDMA). CCPS can encapsulate low-dose doxorubicin hydrochloride (DOX) to induce immunogenic cell death (ICD) and 2-(1-hexyloxyethyl)-2-devinyl pyropheophorbide-a (HPPH), a photosensitizer to facilitate photodynamic therapy (PDT) for reactive oxygen species (ROS) generation. This combination is able to enhance the population of TAAs and DC recruitment, eliciting an immune response cascade. In addition, CCPS with primary and tertiary amines act as adjuvant, both of which can stimulate DCs recruited to form an *in situ* DC vaccine after combination with TAAs for MC38 colorectal cancer treatment. *In vivo* results indicate that the all-in-one polymersomal nanoformulation (CCPS/HPPH/DOX) increases mature DCs in tumor-draining lymph nodes (tdLNs) and $CD8^+$ T cells in tumor tissues to inhibit primary and distant MC38 tumor growth following a single intravenous injection with a low dose of DOX and HPPH.**

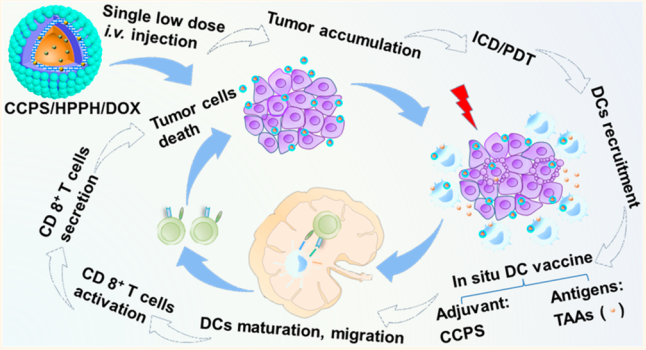

KEYWORDS: *immunogenetic cell death, photodynamic therapy, polymersomes as adjuvant, in situ DC vaccine, colorectal cancer immunotherapy*

A cancer vaccine is one of three key approaches in cancer immunotherapy along with immune checkpoint blockade therapy and adoptive T cell therapy.[1−7] Due to the critical role of dendritic cells (DCs) in provoking T cells, many studies have concentrated on a DC vaccine for cancer immunotherapy.[8,9] For example, Sipuleucul-T, a DC-based therapeutic cancer vaccine, received U.S. Food and Drug Administration (FDA) approval in 2010 for the treatment of metastatic castrate-resistant prostate cancer.[2] For these conventional DC vaccines, DCs are extracted from the patient's blood by leukapheresis and conditioned with antigens and adjuvants before reinfusion into the host.[9] Therefore, a smart cancer vaccine that minimizes the handling of blood products and offers superior immune response and antitumor efficacy is desirable.

Nanotechnology represents an efficient platform for the design of a cancer vaccine.[10−17] After systemic administration, nanoparticles can preferentially accumulate in tumor tissues due to the enhanced permeability and retention (EPR) effect.[18,19] Chen *et al.* used poly(lactic-*co*-glycolic) acid (PLGA) nanoparticles to encapsulate the photothermal agent indocyanine green (ICG) and the toll-like-receptor-7 (TLR-7) agonist imiquimod (as adjuvant) combined with secreted tumor-associated antigens (TAAs) forming a cancer vaccine after

Received: November 1, 2018
Accepted: March 5, 2019
Published: March 5, 2019

DOI: 10.1021/acsnano.8b08346
ACS Nano 2019, 13, 3083−3094

Scheme 1. Schematic Illustration of an *in Situ* DC Vaccine Exploiting Chimeric Cross-Linked Polymersomes (CCPS)) as Adjuvant Combined with Tumor-Associated Antigens (TAAs)) Induced by PDT and ICD for MC38 Colorectal Cancer Immunotherapy. (a) Self-Assembly of the Versatile Copolymer for an All-in-One Polymersomal Nanoformulation Encapsulating HPPH and DOX. (B) Immune Response Cascade after Injection of CCPS/HPPH/DOX with Laser Irradiation for *in Situ* DC Vaccine Formation, CD 8^+ T Cell Activation, AAnd Tumor Cell Death.

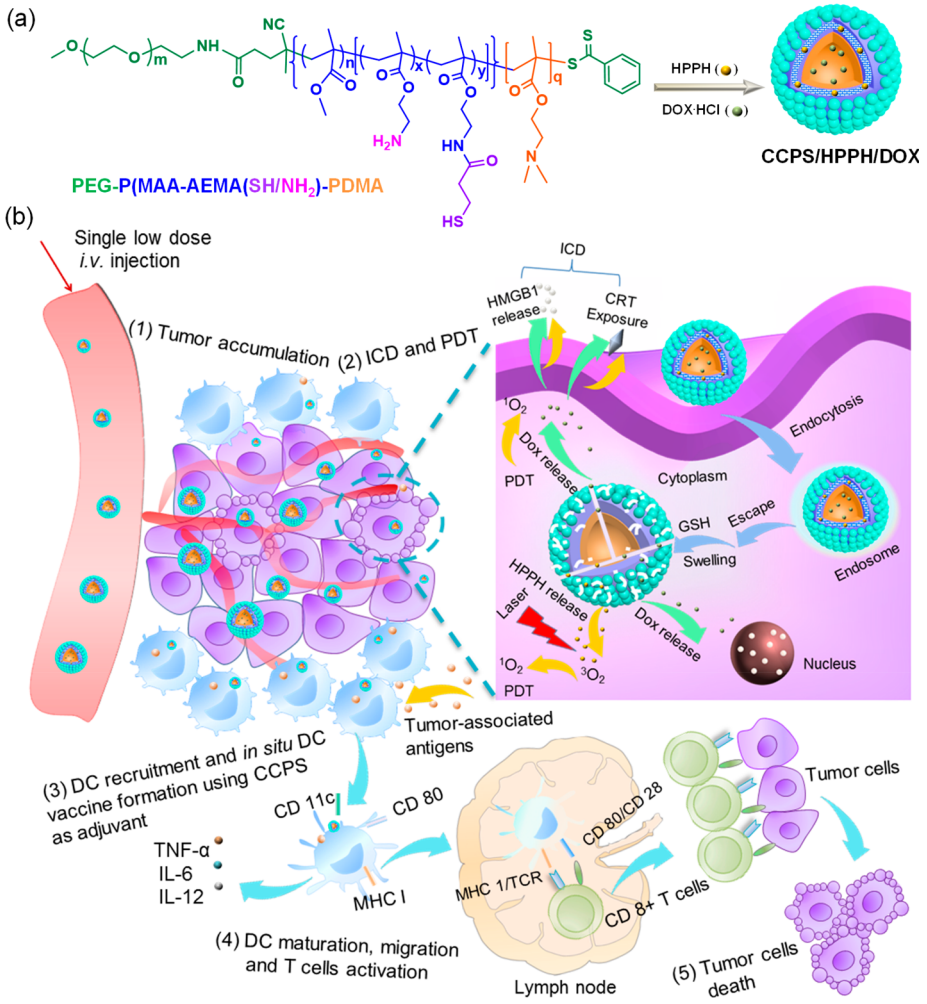

photothermal ablation of a tumor.[20] However, multiple injections and relatively high drug doses are needed for effective treatment efficacy in many studies.[21−24] It is thus essential to develop nanoformulas that simultaneously target multiple pathways for enhanced therapeutic efficacy. Ideally, this should be accomplished with a single low-dose injection without the need of additional adjuvant administration.

Chemotherapeutic agents (*e.g.*, doxorubicin, mitoxanthrone, oxaliplatin), photodynamic therapy (PDT), photothermal therapy (PTT), and radiotherapy (RT) can cause immunogenic cell death (ICD) with high mobility group box 1 (HMGB1) release and calreticulin (CRT) exposure.[25−30] Liu *et al.* demonstrated that reducing Wnt family member 5A protein by means of a trimeric protein trap can remodel the immunosuppressive tumor microenvironment of melanoma to confer increased sensitivity to doxorubicin (DOX).[31] PDT mediated by photosensitizers such as 2-(1-hexyloxyethyl)-2-devinyl pyropheophorbide-a (HPPH), Ce6, and porphyrin can cause tumor cell death, leading to increased antigen spread.[29,32−36] PDT can also induce ICD and inflammation to further recruit DCs to the tumor site.[2,26] Moreover, it was reported that positively charged polymers containing primary, secondary, or tertiary amines could serve as adjuvants possibly because the protonated amines could cause endo/lysosomal membrane disruption and pro-inflammation factor release or a stimulator of interferon genes (STING)-dependent pathway.[37−41] It was reported that particles could cause NLRP3 inflammasome activation and IL-1β secretion after cellular internalization and escape from endosome.[37,39,42] This process mainly induces endosome membrane destruction, cathepsin B release, and K^+ efflux, which plays a key role in inflammation activation of the host. Li *et al.* reported mesoporous silica microrods with adsorbed polyethylenimine (PEI) as adjuvant could serve as a cancer vaccine after neoantigen encapsulation.[37]

Herein, we report chimeric cross-linked polymersomes (CCPS) with co-encapsulation of DOX and HPPH (CCPS/HPPH/DOX) to form an *in situ* DC vaccine using copolymers as adjuvant combined with TAAs for MC38 colorectal cancer treatment (Scheme 1). Polymersomes have been widely used in the biomedical field due to their good stability, adjustable properties, and diversity in polymer structure constituents.[43−50] We designed a copolymer, polyethylene glycol-poly(methyl methyacrylate-*co*-2-amino ethyl methacrylate (thiol/amine))-poly 2-(dimethylamino)ethyl methacrylate (PEG-P(MMA-*co*-

DOI: 10.1021/acsnano.8b08346
ACS Nano 2019, 13, 3083−3094

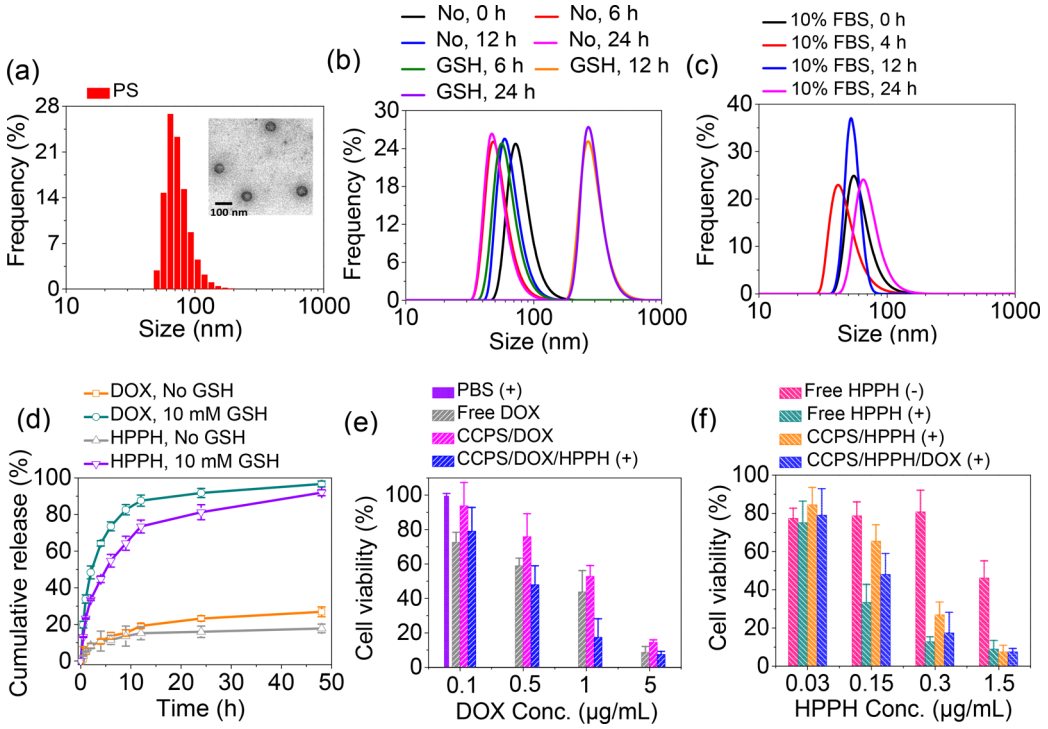

Figure 1. Characterization of chimeric cross-linked polymersomes (CCPS). (a) Size and size distribution of CCPS by DLS (inset: structure characterization by TEM). (b) Size change of CCPS in the presence or absence of 10 mM GSH in PBS within 24 h. (c) Cross-linked stability of CCPS in PBS containing 10% FBS in 24 h. (d) *In vitro* DOX and HPPH release from CCPS nanoformulation with 10 mM or without GSH treatment in PBS within 48 h (n = 3). Cytotoxicity test for MC 38 cells treated by DOX (e) and HPPH (f) formulations first for 24 h of incubation and replaced with fresh medium for laser irradiation at 671 nm (100 mW/cm^2, 1 min) followed by another 24 h of incubation. PBS (+) (e) represents cytotoxicity of only laser irradiation (671 nm, 100 mW/cm^2, 1 min) for MC38 cells. Data are presented as the mean ± SD (n = 4).

AEMA (SH/NH$_2$)-PDMA), that could self-assemble to form asymmetric multifunctional polymersomes after loading DOX and HPPH. Longer PEG chains cover the outer hydrophilic shell to improve bioavailability, and shorter PDMA makes up the inner lumen to enable loading of DOX and also serves as an adjuvant.[38,51] The middle hydrophobic membrane is composed of thiol and amine groups. The thiol groups create the cross-linked structure for stability, prevent drug leakage, and serve as responsive elements for glutathionine (GSH).[52,53] The amine groups aid in HPPH loading efficiency through electrostatic interaction and also contribute as the primary adjuvant load.

RESULTS AND DISCUSSION

Synthesis of Copolymer and Preparation of CCPS. To obtain PEG-P(MMA-*co*-AEMA (SH/NH$_2$)-PDMA, we synthesized PEG-CPPA by amidation reaction and PEG-P(MMA-*co*-BAEMA)-PDMA using reversible addition−fragmentation chain transfer (RAFT) polymerization separately and characterized them by ^{1}H NMR spectra (Figure S1 and Figure S5). 4-Cyano-4-(phenylcarbonothioylthio)pentanoic acid *N*-succinimidyl ester (CPPA) is a versatile RAFT agent, and PEG-P(MMA-*co*-BAEMA)-PDMA is a precursor containing *tert*-butyloxycarbonyl (BOC) protecting groups. Figure S1 and Figure S5 show the degree of CPPA substitution was 94% and that the molecular weight of PEG-P(MMA-*co*-BAEMA)-PDMA was 5.0-(3.2-*co*-11.2)-1.8 kg·mol^{-1}. The BOC protecting groups were removed by treating the polymer with trifluoroacetic acid (Figure S6).[54] We then characterized the copolymer after amidation with mercaptopropionic acid by ^{1}H NMR (Figure S7) and the TNBSA method.[55,56] Our data showed that an average of 21 thiol and 22 amine groups were present in each polymer chain (Figure S8). The copolymer self-assembled to form CCPS in phosphate-buffered saline (PBS; 10 mM, pH 7.4, 150 mM NaCl), resulting in hollow structures that had an average particle size of 70 nm (Figure 1a). As controls, we also synthesized three different copolymers without amines or thiols (Figures S2, S4, and S5). We obtained two symmetric polymersomes with copolymers PEG-P(MMA-*co*-BAEMA) (PS) and PEG-P(MMA-*co*-AEMA(NH$_2$/SH) (PS/NH$_2$) that had average particle sizes of 125 and 174 nm, respectively (Figure S9a,b and Table S1). We also prepared asymmetric polymersomes with an average particle size of 92 nm using copolymer PEG-P(MMA-*co*-BAEMA)-PDMA (PS/PDMA) (Figure S9c and Table S1).

Reduction Responsiveness and Cross-Linker Stability of CCPS and *in Vitro* Drug Release from CCPS/HPPH/DOX. Figure 1b revealed that CCPS size increased to 300 nm in the presence of 10 mM GSH at 12 h. However, the size remained virtually unchanged for CCPS without GSH treatment even after 24 h of incubation because of the presence of stable cross-linkers. Moreover, nearly no size change was observed for CCPS in a shaking bath (37 °C, 200 rpm) within 24 h (Figure S9d). Nevertheless, the size increased to 1000 nm in 24 h for non-cross-linked polymersomes (PS/PDMA) (Figure S9d). CPPS also retained good stability in PBS containing 10% fetal bovine serum (FBS) (Figure 1c). After co-encapsulation of DOX and HPPH, the particle size was 86 nm with loading contents of 9.03% and 5.49%, respectively. The zeta potential was measured close to a neutral charge (Table S3). With 10 mM GSH, almost all DOX and HPPH molecules were released from polymer-

DOI: 10.1021/acsnano.8b08346
ACS Nano 2019, 13, 3083−3094

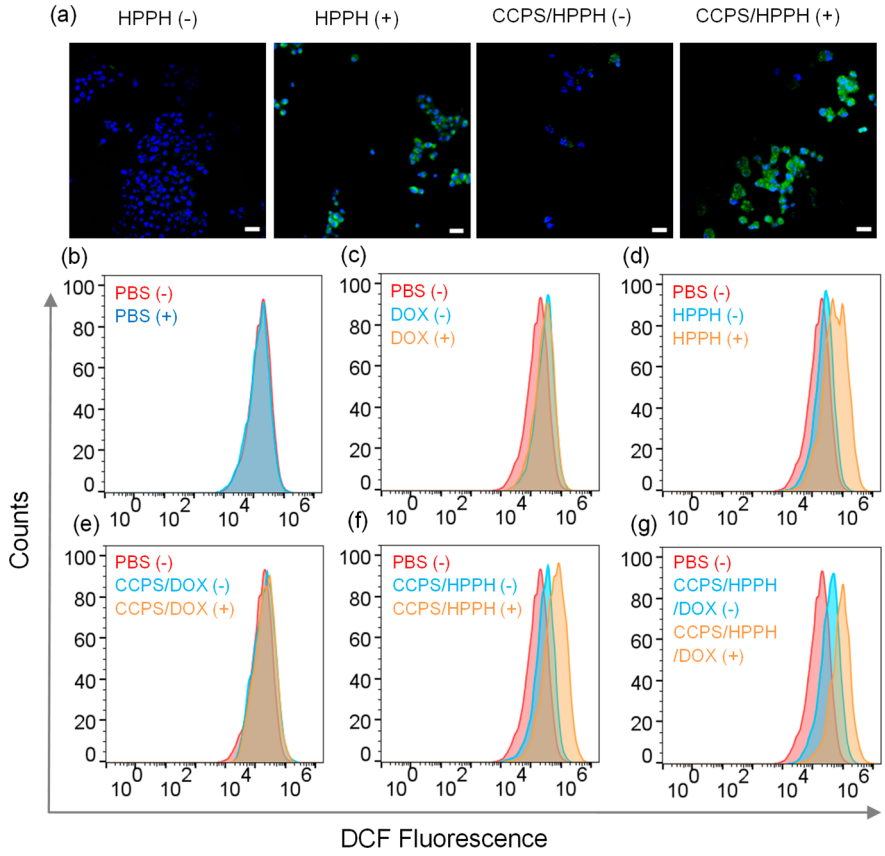

Figure 2. ROS generation in MC38 cells after different formulation treatment using DCFH-DA as a fluorescence probe. (a) MC38 cells treated by free HPPH and CCPS/HPPH with laser irradiation at 671 nm (100 mW/cm^2, 1 min) characterized *via* CLSM. Cell nuclei were stained with DAPI (blue). Green shows DCF fluorescence. Scale bars: 40 μm. (b−g) Cells treated by different formulations with or without laser irradiation at 671 nm (100 mW/cm^2, 1 min) *via* flow cytometry characterization.

somes within 48 h as the disulfide bonds are reduced to thiols, leading to polymersome swelling and drug release (Figure 1d). Without GSH, only 23% DOX and 18% HPPH were released at the same time point.

Cytotoxicity, ROS Generation, and ICD of CCPS/HPPH/DOX for MC38 Cells. We first investigated the cytotoxicity of the polymersomal nanomedicine on MC38 colorectal cancer cells. DOX inhibits topoisomerase II progression by intercalating DNA,[57] while HPPH causes cell death by intracellular ROS generation after laser irradiation.[58] Treatment of CCPS/HPPH/DOX with laser irradiation showed a greater decrease in cell viability compared with the other control nanoformulations (Figure 1e,f). In addition, laser irradiation only was nearly nontoxic (Figure 1e). Figure S10a results demonstrated that CCPS alone was rarely nontoxic to MC38 cells, showing good biocompatibility. Due to the lower GSH concentration in DC2.4 cells than that in tumor cells, which may cause less release of drugs from CCPS, higher cell viability was observed for DC2.4 cells treated by CCPS/HPPH/DOX even after laser irradiation (Figure S10b). Without laser irradiation, CCPS/HPPH/DOX revealed very weak cytotoxicity to DC2.4 cells (Figure S10b). We used 2′,7′-dichlorofluorescin diacetate (DCFH-DA) as a fluorescence probe to measure ROS levels in MC38 cells after treatment by HPPH and CCPS/HPPH with laser irradiation (Figure 2a and Figure S11) by confocol laser scanning microscopy (CLSM). Without laser irradiation, minimal fluorescence was observed. DCF fluorescence intensity was quantified by flow cytometry (Figure 2b−g). We observed a 4.8−5.3-fold increase in fluorescence signal intensity for free HPPH, CCPS/HPPH, and CCPS/HPPH/DOX after laser irradiation compared to their respective controls without laser irradiation. For cells treated with DOX formulations, no fluorescence shift was observed even after laser irradiation.

Next, we studied HMGB1 release by the enzyme-linked immunosorbent assay (ELISA) and CRT exposure by CLSM and flow cytometry in MC38 colon cancer cells following ICD induction by DOX and PDT. HMGB1 release from MC38 cells increased from 1.7- to 2.7-fold after incubation with different DOX and HPPH formulations with laser irradiation compared with the PBS group (Figure S12). Both DOX and PDT induced significant CRT exposure for MC38 cells, as confirmed by the CLSM results (Figures 3a,b, S13 and S14). Quantification of the flow cytometry results showed a 4.7−5.1-fold increase in CRT antibody fluorescence after DOX and HPPH formulation treatment compared to the PBS group (Figure 3c,d). These results reaffirmed that both DOX and PDT can cause ICD.

DC2.4 Cell Maturation Using CCPS as Adjuvant. To study whether positively charged polymers containing tertiary and primary amines could serve as adjuvants, we investigated the DC maturation stimulated by different polymers with or without amines. Using DC2.4 cells, we used CD11c and CD80 as the maturation and costimulation markers. According to Figure 4a, polymersomes containing both PDMA (tertiary amine) and primary amine induced the most DC maturation, with $CD11c^+$ and $CD80^+$ cell population as high as 17.6%, compared with PBS (0.35%), PS (2.04%), PS (NH_2) (1.73%), and PS (PDMA) (3.44%). Note that the polymersome with tertiary and Boc protected primary amine was also able to induce DC maturation

DOI: 10.1021/acsnano.8b08346
ACS Nano 2019, 13, 3083−3094

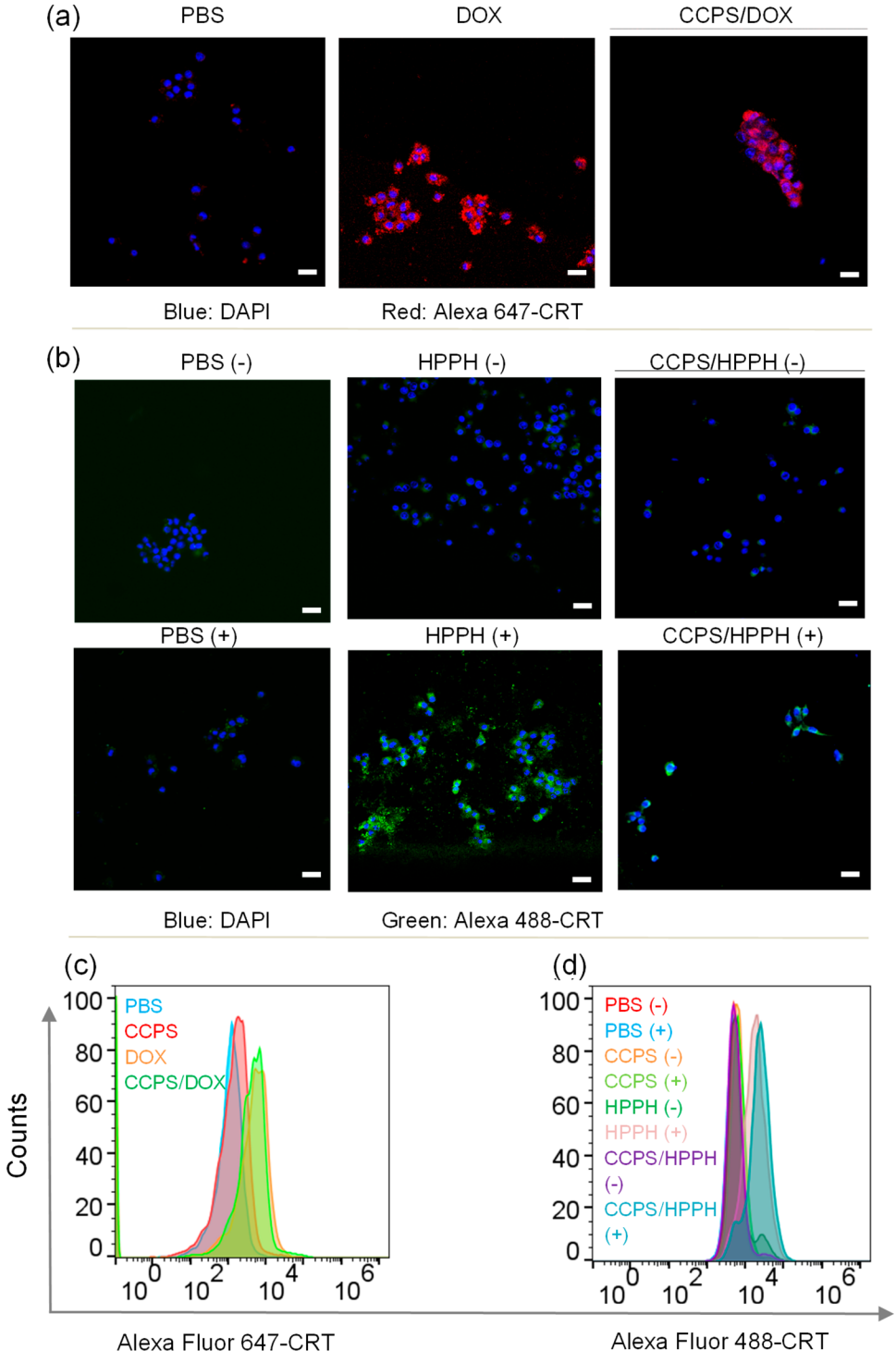

Figure 3. Immunogenic cell death (ICD) of MC38 cells measured by CRT exposure after treatment with different drug formulations. (a) DOX and CCPS/DOX treatment by CLSM characterization. Cell nuclei were stained with DAPI (blue) and CRT was stained by anti-Alexa Fluor 647-CRT (red). (b) HPPH and CCPS/HPPH treatment after laser irradiation at 671 nm (100 mW/cm^2, 1 min) by CLSM characterization. Cell nuclei were stained with DAPI (blue) and CRT was stained by anti-Alexa Fluor 488-CRT (green). Scale bars: 40 μm. (c) DOX formulations stained with anti-Alexa Fluor 647-CRT and (d) HPPH formulations stained with anti-Alexa Fluor 488-CRT with or without laser irradiation at 671 nm (100 mW/cm^2, 1 min) *via* flow cytometry characterization.

to some extent, most likely due to partial hydrolysis of the Boc protecting group to the amine within lysosomes.

Enhanced Antigen Cross-Presentation for DC2.4 Cells after Co-incubation with OVA and CCPS. We next investigated whether co-incubation with CCPS and ovalbumin (OVA) could elicit antigen cross-presentation by measuring cell surface expression of CD11c and SIINFEKL/H-2K^b. DC2.4 cells treated by CCPS and OVA had 20.3% coexpression of CD11c and SIINFEKL/H-2K^b, about 19-fold and 63-fold higher than the OVA group and PBS group, respectively (Figure 4b). Therefore, the adjuvant function of CCPS played a crucial part in DC maturation and antigen cross-presentation.

DOI: 10.1021/acsnano.8b08346
ACS Nano 2019, 13, 3083−3094

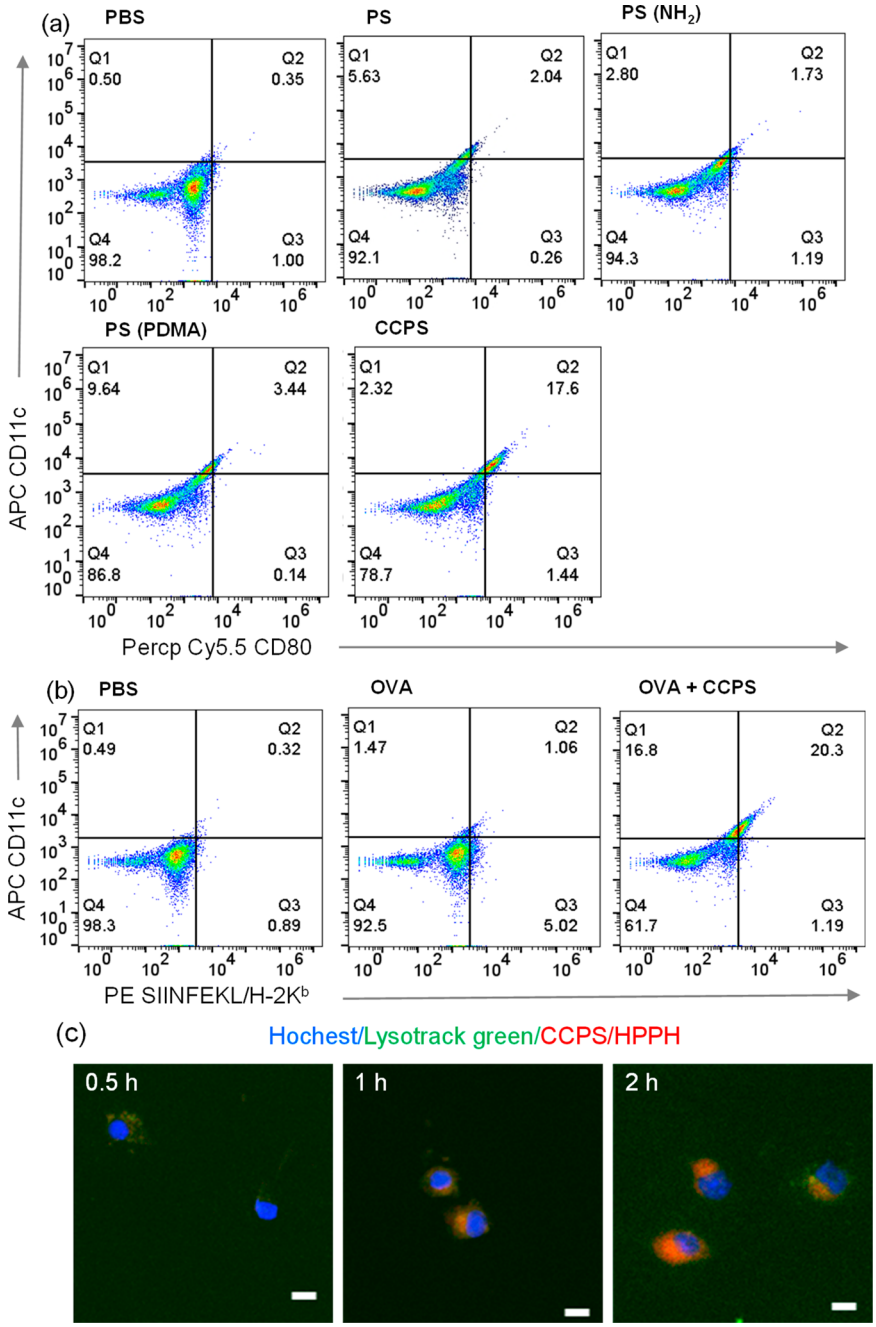

Figure 4. (a) DC2.4 cell maturation after treatment by PS, PS (NH_2), PS (PDMA), and CCPS. CD80 and CD11c as markers stained with Percp Cy5.5 anti-CD80 and APC anti-CD11c, respectively. (b) DC 2.4 cell cross-presentation by co-incubation of CCPS as adjuvant and OVA. MHC I single-chain H-2K^b stained with PE anti-SIINFEKL/H-2K^b and CD11c stained with APC anti-CD11c. Cells treated by OVA or PBS alone served as controls. (c) Endosome escape of CCPS/HPPH from DC2.4 cells after 0.5, 1, and 2 h of incubation. Cell nuclei were stained with Hochest (blue), endosome was stained by Lysotrack Green (green), and red fluorescence was HPPH. Scale bars: 15 μm.

Mechanism Investigation for CCPS as Adjuvant. We then investigated the endo/lysosomal escape of CCPS/HPPH from DC2.4 cells. Results from Figures 4c and S15 demonstrated that CCPS/HPPH could quickly escape from the endosomes even within 0.5 h with nearly no observation of colocalization between Lysotracker green and red HPPH. When incubation time was prolonged to 1 and 2 h, the red HPPH fluorescence intensity increased; however, still very little colocalization was observed. This suggests that the nanoparticles had strong endosome escapability, which probably helped to release pro-inflammation factors for adjuvant function.

***In Vivo* Immune Stimulation of CCPS/HPPH/DOX.** Prompted by the promising *in vitro* results, we proceeded to study the *in vivo* immunostimulation for MC38 tumor bearing C57BL/6 mice after different nanoformulation treatment. Tumor-bearing mice treated by CCPS/HPPH/DOX after laser irradiation (671 nm, 200 mW/cm^2, 10 min) had the highest IL-6, IL-12, and TNF-α levels in peripheral blood serum on day 3 after injection as compared with the other groups. This corresponded to 4−9-fold higher than PBS and free DOX and 2−3-fold higher than CCPS/DOX and CCPS/HPPH groups (Figure 5a). ICD induced by the combination of DOX and

DOI: 10.1021/acsnano.8b08346
ACS Nano 2019, 13, 3083−3094

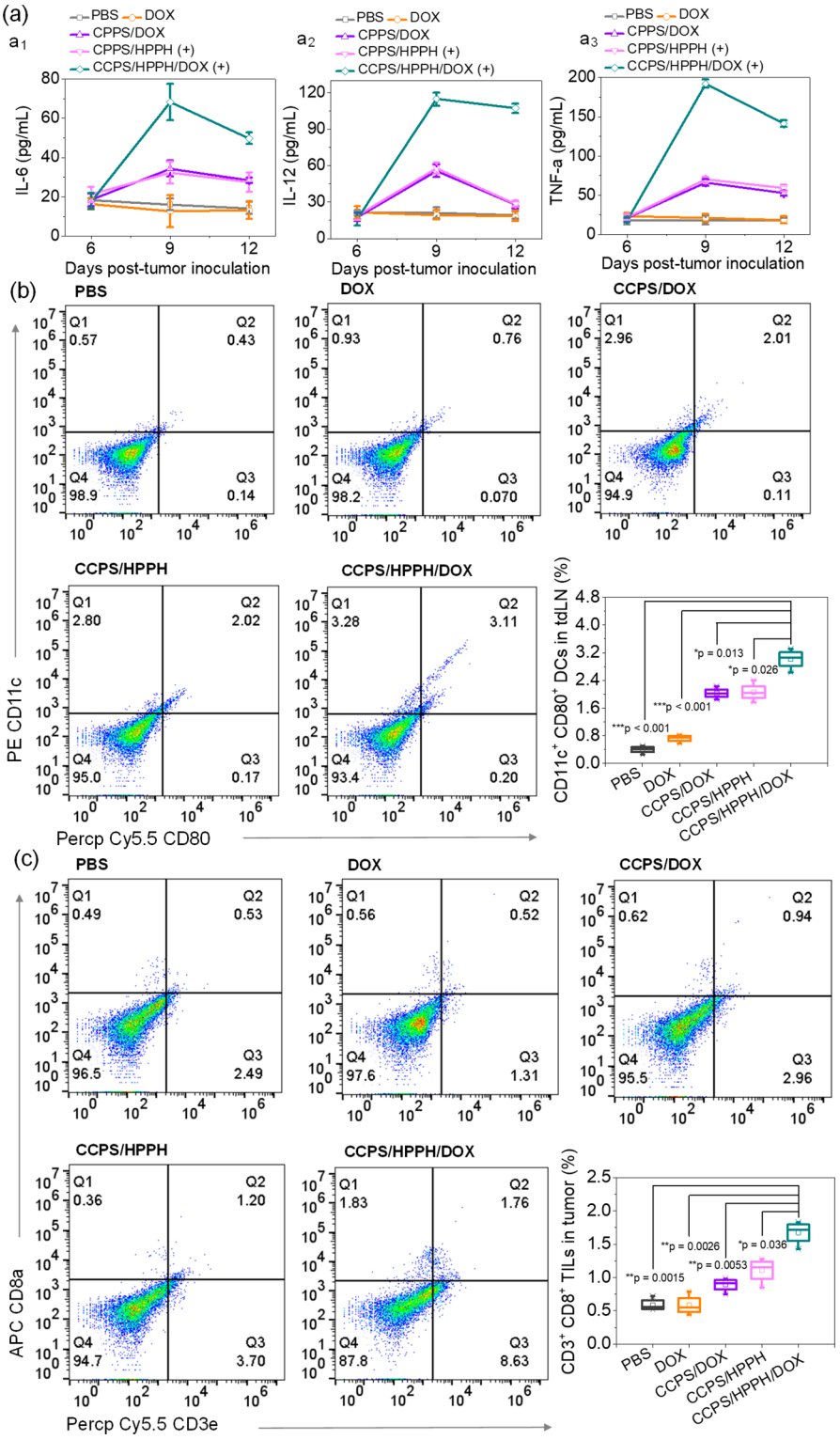

Figure 5. ***In vivo*** **immune stimulation. (a) Cytokine IL-6 (a_1), IL-12 (a_2), and TNF-α (a_3) levels in peripheral blood serum after treatment. On day 6 post-tumor inoculation, mice were injected by i.v. with different formulations and irradiated 24 h later for CCPS/HPPH and CCPS/HPPH/DOX groups at 671 nm (200 mW/cm^2, 10 min) ($n = 3$). (b) Activated DC ratio in tumor-draining lymph nodes (tdLNs) for mice treated with different nanoformulations ($n = 3$). Percp Cy5.5 anti-CD80 and PE anti-CD11c stained with CD80 and CD11c markers in DCs. (c) Tumor infiltrating lymphocytes in tumor sites after treatment ($n = 3$). CD3e and CD8a as markers on CD 8$^+$ T cell surfaces stained with APC anti-CD8a and Percp Cy5.5 anti-CD3e. (Statistical analysis: one-way ANOVA with Tukey's multiple comparison tests; *$p < 0.05$, **$p < 0.01$, ***$p < 0.001$.) Data are presented as the mean ± SD.**

PDT, or PDT alone for the inflammation, could promoted DC maturation and cytokine secretion. We observed around 3.02% activated DCs in tumor-draining lymph nodes (tdLNs) for mice after CCPS/HPPH/DOX treatment with laser irradiation (671 nm, 200 mW/cm^2, 10 min) on day 6 post-injection (Figure 5b). The values for mice treated by PBS, DOX, CCPS/DOX, and

DOI: 10.1021/acsnano.8b08346
ACS Nano 2019, 13, 3083−3094

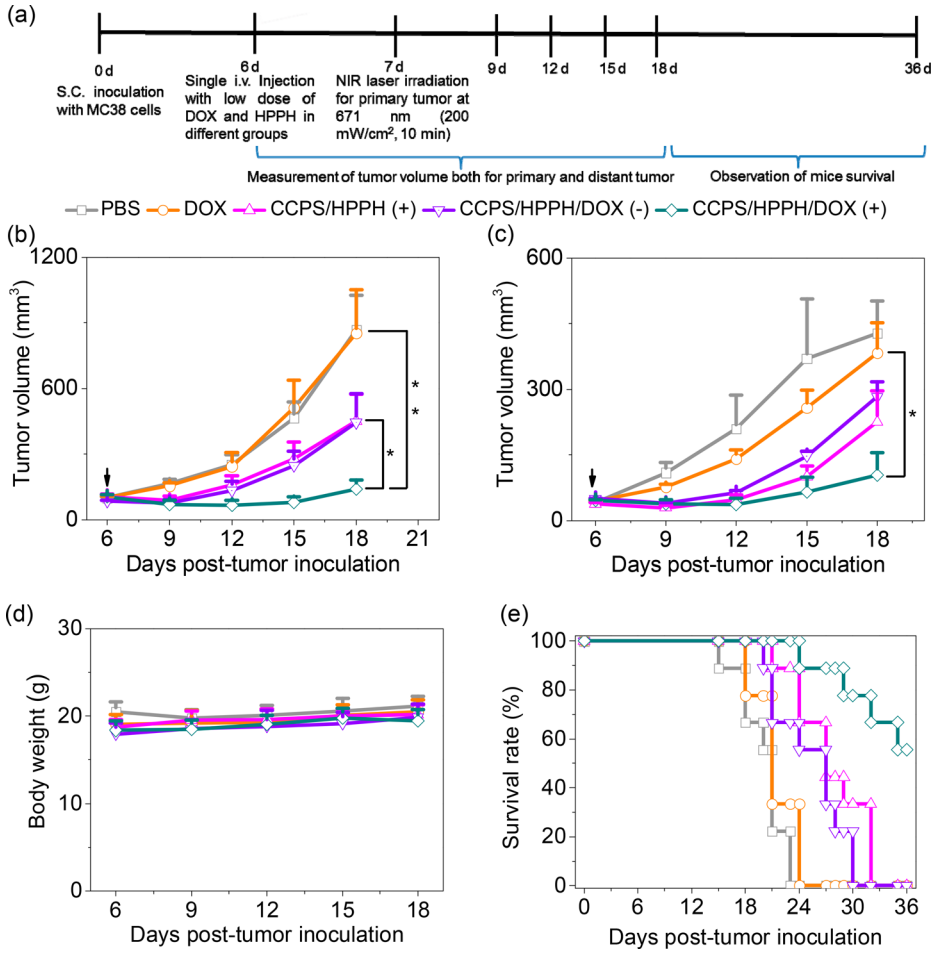

Figure 6. ***In vivo*** **antitumor efficacy of different nanoformulations for MC38 tumor-bearing C57BL/6 mice. (a) Schematic illustration of CCPS/HPPH/DOX based on PDT and ICD for TAA secretion by dying tumor cells and combining with CCPS as adjuvant for** ***in situ*** **DC vaccination to inhibit MC38 tumor growth and abscopal effect. (b) Tumor volume changes of primary (b) and distant tumors (c) treated with different formulations within 18 d (n = 9). (Statistical analysis: one-way ANOVA with Tukey's multiple comparisons; *p < 0.05, **p < 0.01.) (d) Body weight changes for mice within 18 d. (e) Survival curves of mice in each group after treatment. Data are presented as the mean ± SD.**

CCPS/HPPH groups were lower at 0.41%, 0.72%, 2.03%, and 2.06%, respectively (Figure 5b). There was no noticeable increase in the population of mature DCs and $CD8^+$ T cells in the spleen, and also no apparent damage to other major organs was observed from hematoxylin and eosin (H&E) results, suggesting low systemic toxicity (Figures S16a,b and S17). Since cytotoxic T lymphocytes are responsible for exerting cytocidal effects, we investigated the tumor infiltrating lymphocyte (TIL) populations in whole tumor tissues. There was approximately 1.7% TILs in tumor tissues for mice treated by CCPS/HPPH/DOX with laser irradiation (671 nm, 200 mW/cm^2, 10 min) on day 6 post-injection, which was 1.5- to 1.8-fold higher than those in the CCPS/DOX and CCPS/HPPH groups (Figure 5c).

Prominent *in Vivo* Antitumor Activities and Abscopal Effect of CCPS/HPPH/DOX. To investigate the *in vivo* therapeutic behavior, we studied immunotherapy efficacy for mice bearing primary and distant tumors. C57BL/6 mice (6–8 weeks) were subcutaneously inoculated with 6.0×10^5 MC38 cancer cells in the right flank (primary tumor) and 2.0×10^5 MC38 cancer cells in the left flank (distant tumor) (Figure 6a). The mice were randomly divided into five groups (n = 9) on day 6 post-tumor inoculation when tumors of the right side reached 100 mm^3. For treatment, we administered a single intravenous injection of low-dose DOX (0.5 mg/kg) and HPPH (0.3 mg/kg). The tumors were significantly inhibited within 18 days for mice treated with CCPS/HHPH/DOX with the following laser irradiation (671 nm, 200 mW/cm^2, 10 min) for primary tumors 24 h after injection (Figure 6b). Nevertheless, tumors still grew slowly for mice treated with CCPS/HPPH/DOX without laser irradiation (Figure 6b). As for the CCPS/HPPH group, tumor growth was inhibited to some degree due to photodynamic immunotherapy (Figure 6b). However, the efficacy was limited since DOX was omitted. Primary tumor volumes increased quickly for the PBS and DOX groups within 18 d (Figure 6b). Moreover, we observed a significant abscopal effect for the tumor inhibition of distant tumors for mice treated with CCPS/HPPH/DOX (Figure 6c). At 18 d after tumor inoculation, no apparent body weight changes were observed, indicating good biocompatibility of nanoformulations or adverse effects of free DOX at the selected dose level (Figure 6d). All the mice treated by free DOX and PBS were euthanized in 24 and 23 d, respectively, because of tumor size or ulceration. The median survival for PBS and DOX groups was 21 d. The median survival for mice treated with CCPS/HPPH with laser irradiation and CCPS/HPPH/DOX without laser irradiation was 27 d. However, over half of the mice treated by CCPS/HPPH/DOX with laser irradiation still survived even 36 d post-tumor

DOI: 10.1021/acsnano.8b08346
ACS Nano 2019, 13, 3083–3094

inoculation (Figure 6e). Collectively, our data show good tumor inhibition efficacy of CCPS/HPPH/DOX after laser irradiation.

CONCLUSIONS

This study reported an *in situ* formed DC vaccine using multifunctional polymersomes as adjuvant combined with chemotherapy and PDT. Owing to the small size, good cross-linked stability, and superior loading content, CCPS/HPPH/DOX demonstrated high cytotoxicity. Both DOX and PDT induced ICD, causing HMGB1 release and CRT exposure, and PDT also generated intracellular ROS. The embedded amine groups served as adjuvant for DC maturation and helped antigen cross-presentation after combination with OVA. *In vivo*, CCPS/HPPH/DOX induced high cytokine levels in serum, more expression of mature DC in tdLNs and TILs in tumor tissue, and prominent immunotherapy efficacy for primary and distant tumors even with low drug dose after a single injection. In addition, the increased expression of CD80 on the DC surface predicts that the *in situ* DC vaccine will likely enhance antitumor efficacy after combination with anti-CTLA-4 for costimulatory signal increment between CD80 and CD28 in T cells. Meanwhile, the vaccine nanotechnology may attenuate T cell exhaustion when combined with anti-PD-1 to block the PD-1/PD-L1 pathway. Overall, we hope the design will inspire scientific researchers in cancer therapy.

METHODS

Synthesis of PEG-P(MMA-*co*-AEMA(NH_2/SH))-PDMA. We first synthesized copolymer PEG-P(MMA-*co*-BAEMA)-PDMA by RAFT polymerization using AIBN as the initiator.[59] Simply, PEG-CPPA (100 mg, 0.02 mmol), monomer MMA (120 mg, 1.2 mmol), BAEMA (275 mg, 1.2 mmol), and AIBN (0.49 mg, 0.003 mmol) were weighed and added into a flask with stirring to dissolve in 1,4-dioxane (5 mL) completely. After nitrogen inlet under the surface for about 40 min, the flask was sealed and moved to an oil bath at 70 °C for 2 d. Then, the third monomer, DMA (60 mg, 0.38 mmol), and AIBN (0.164 mg, 0.001 mmol) were added under nitrogen for another 2 d of reaction in a 70 °C oil bath. PEG-P(MMA-*co*-BAEMA) could be obtained after precipitation in cold ether, and the molecular weight of this copolymer was determined by ^{1}H NMR spectrum.

PEG-P(MMA-*co*-BAEMA)-PDMA was able to hydrolyze completely to PEG-P(MMA-*co*-AEMA(NH_2))-PDMA in the presence of trifluoroacetic acid (TFA) for Boc group removal.[54] Briefly, PEG-P(MMA-*co*-BAEMA)-PDMA (500 mg, 0.024 mmol) was first dissolved in DCM (2 mL), and 2 mL of TFA was added. After 2 h of stirring, all the Boc groups disappeared, which was verified by ^{1}H NMR spectrum for the absent peak at δ 1.4 ppm. Mercaptopropionic acid (MPA) (31.8 mg, 0.3 mmol) was first activated by NHS (35.0 mg, 0.3 mmol) and EDC (93.1 mg, 0.6 mmol) in DCM (2 mL) for 2 h at room temperature (rt). The above product was added to PEG-P(MMA-*co*-AEMA(NH_2))-PDMA (200 mg, 0.012 mmol) and a DMF (2 mL) solution to react for another 24 h at rt for PEG-P(MMA-*co*-AEMA(NH_2/SH))-PDMA. The SH content was calculated in every chain from the ^{1}H NMR spectrum and amine content in every chain by the TNBSA assay.[55,56]

Preparation of Chimeric Cross-Linked Polymersomes and Drug Loading for CCPS/HPPH/DOX. CCPS were prepared by the solvent exchange method. Briefly, 50 μL of copolymer PEG-P(MMA-*co*-AEMA (NH_2/SH))-PDMA solution in dimethylformide (DMF) (5 mg/mL) was added slowly to 950 μL of PBS (10 mM, pH 7.4, 150 mM NaCl) from the bottom and allowed to stand for 20 min followed by slight rotation. After that, we could get the uniform polymersomes when DMF was removed after dialysis (MWCO, 3500) in PBS (10 mM, pH 7.4, 150 mM NaCl), simultaneously getting cross-linked polymersomes for the oxygen in the media. The size, size distribution, and zeta potential were measured by dynamic light scattering (DLS). Polymersomes self-assembled from other control copolymers were acquired by similar methods. CCPS loaded with HPPH and DOX (CCPS/HPPH/DOX) were prepared by a similar approach to the above. In short, 50 μL of copolymers in DMF (5 mg/mL) was first mixed with HPPH in DMSO followed by addition to a premixed DOX solution in PBS (10 mM, pH 7.4, 150 mM NaCl). After standing for 20 min and slow rotation, we obtained CCPS/HPPH/DOX, unloaded drugs, and organic solvent, which were removed after dialysis, and cross-linked structures for the existing oxygen in the media. Drug loading content and drug loading efficiency were measured by UV−vis.

ROS Generation by PDT. We used DCFH-DA as a fluorescence probe to detect intracellular ROS generation of MC38 cells and verified it by CLSM and flow cytometry. By CLSM, 2.0×10^4 MC38 cells were seeded in eight-well plates supplemented with DMEM media with 10% FBS and 1% penicillin and streptomycin. After 24 h of culture, free HPPH and CCPS/HPPH ($n = 2$) were added, respectively. In the next 4 h of incubation, DCFH-DA was added and incubated for 0.5 h. Next, one of these in every group underwent laser irradiation at 671 nm (100 mW/cm^2, 1 min). Following media aspiration and PBS (×3) washing, cells were fixed by Z-fix solution for 15 min. After washing three times with PBS, cell nuclei were stained by DAPI (5 μg/mL) for 10 min, washed again with PBS (×3), and covered by a coverslip and nail polish. Images were obtained in a confocol laser scanning microscope (Zeiss LSM 780).

We then quantitated it by flow cytometry. Briefly, 5.0×10^5 MC38 cells were seeded in six-well plates containing DMEM media with 10% FBS and 1% penicillin and streptomycin. On the second day, free DOX, HPPH, CCPS/DOX, CCPS/HPPH, and CCPS/HPPH/DOX ($n = 2$) were added for a further 4 h incubation. Before laser irradiation at 671 nm (100 mw/cm^2, 1 min), DCFH-DA was first co-incubated with every group for 0.5 h. After laser irradiation, cells were digested by trypsin, washed with PBS (×3), suspended in PBS, and tested by flow cytometry.

ICD Induced by CPPS/HPPH/DOX for CRT Exposure. As for CRT exposure, we characterized it by CLSM and flow cytometry, separately. For the CLSM characterization and induction by DOX, 2.0×10^4 MC38 cells were first seeded in eight-well plates filled with 400 μL of DMEM media with 10% FBS and 1% penicillin and streptomycin. After 24 h of culture, 100 μL of CCPS, free DOX, and PS/DOX were added separately. PBS and CCPS groups served as a control. After a further 24 h of incubation, media were aspirated, cells were washed with PBS (×3), and anti-Alexa Fluor 647-CRT was added to stain the exposed CRT according to the manufacturer's protocol. Following PBS washing (×3), cells were fixed by Z-fix solution for 15 min. After another PBS washing (×3), cells were stained with DAPI (5 μg/mL) for 10 min. After PBS washing (×3), cells were covered by nail polish and photographed by CLSM. For the flow cytometry characterization treated by DOX, 5.0×10^5 MC38 cells were seeded in six-well plates supplemented with DMEM media with 10% FBS and 1% penicillin and streptomycin; DOX and PS/DOX were added after 24 h of culture. After another 24 h of incubation, cells were digested by trypsin and washed three times by PBS. After anti-Alexa Fluor 647-CRT staining for 40 min and PBS washing another three times, all the cells in each group were suspended in 0.5 mL of PBS, respectively, and tested by flow cytometry.

For CRT exposure induced by PDT, the methods were similar to the above. For CLSM charaterization, 2.0×10^4 MC38 cells were seeded in eight-well plates and cultured for a further 24 h. Then, PBS, CCPS, HPPH, and CCPS/HPPH ($n = 2$) were added separately. After 24 h of incubation, all the culture media were replaced with fresh media, and one of each group was irradiated at 671 nm (100 mW/cm^2, 1 min). After another 4 h of incubation, the media were aspirated and cells were washed by PBS, stained with anti-Alexa Fluor 488-CRT, fixed with Z-fix solution, and stained with DAPI similar to the above procedures. The images were acquired by CLSM. For flow cytometry characterization, 5.0×10^5 MC38 cells were seeded in six-well plates supplemented with DMEM media with 10% FBS and 1% penicillin and streptomycin for a further 24 h culture; then PBS, CCPS, HPPH, and CCPS/HPPH ($n = 2$) were added. After 24 h of incubation, one of each group was irradiated at 671 nm (100 mW/cm^2, 1 min). Following a 4 h incubation,

DOI: 10.1021/acsnano.8b08346
ACS Nano 2019, 13, 3083−3094

cells were digested, washed by PBS, stained with anti-Alexa Fluor 488-CRT, suspended in 0.5 mL of PBS, and measured by flow cytometry.

Adjuvant Function of CCPS. Then we investigated the adjuvant property of CCPS by DC maturation and antigen cross-presentation. Briefly, 5.0×10^5 DC 2.4 cells were seeded in six-well plates supplemented with RPMI-1640 media with 10% FBS and 1% penicillin and streptomycin. After 24 h of culture, PS, PS (NH_2/SH), PS (PDMA), and CCPS (NH_2/SH, PDMA) were added separately. The PBS group was a control. After 24 h of incubation, cells were collected and washed with PBS, and stained with APC anti-CD11c and Percp Cy5.5 anti-CD80 according to the manufacturer's protocol. Then, cells were washed with PBS (×3), suspended in 0.5 mL of PBS, and tested by flow cytometry.

We next studied the cross-presentation of CCPS plus OVA. In brief, 5.0×10^5 DC 2.4 cells were first seeded in six-well plates with RPMI-1640 media with 10% FBS and 1% penicillin and streptomycin. After 24 h of culture, OVA and OVA/CCPS were added, respectively, and the PBS group acted as a control. After 24 h of incubation, cells were collected, centrifugated, washed with PBS (×3), and stained with APC anti-CD11c and PE anti-SIINFEKL/H-2Kb according to the manufacturer's protocol. Finally, cells were suspended in 0.5 mL of PBS and measured by flow cytometry.

Endosome Escape of CCPS/HPPH. We characterized the endosome escape of CCPS/HPPH from DC 2.4 cells by CLSM. Simply, 2.0×10^4 DC 2.4 cells were seeded in eight-well plates supplemented with RPMI-1640 media with 10% FBS and 1% penicillin and streptomycin. Following addition of CCPS/HPPH at preset time points, they were incubated for 0.5, 1, and 2 h, respectively. Then, cells were washed with PBS (×3) and endosomes were stained by Lysotracker Green for 40 min. After another PBS washing (×3), nuclei were stained by Hochest for 10 min, washed (×3) again, and covered by a coverslip and nail polish. The images were acquired by CLSM (Zeiss LSM 780).

***In Vivo* Immune Stimulation of CCPS/HPPH/DOX.** We then investigated *in vivo* immune stimulation of CCPS/HPPH/DOX with MC38 tumor bearing C57BL/6 mice (6–8 weeks). First, 6×10^5 MC38 cells were subcutaneously inoculated in the right flank of the mice. On day 6 post-tumor inoculation, they were randomly divided into five groups ($n = 3$) when tumors reached 100 mm^3. Then, PBS, free DOX, CCPS/DOX, CCPS/HPPH, and CCPS/HPPH/DOX were injected by tail vein (DOX: 0.5 mg/kg, HPPH: 0.3 mg/kg) in a single injection. After 24 h, mice treated with CCPS/HPPH and CCPS/HPPH/DOX were laser irradiated at 671 nm (200 mW/cm^2, 10 min). On day 6 post-injection, tumor and tumor-draining lymph nodes were removed from each mouse.

Tumor-Drainging Lymph Node Analysis. Tumor-draining lymph nodes in each group were first cut into small pieces followed by digestion in RPMI-1640 media containing 2% FBS, collagenase (0.5 mg/mL), and DNase (0.1 mg/mL) for 1 h at 37 °C. All the digested suspensions were filtrated, centrifuged, and washed with PBS (×3) followed by staining with PE anti-CD11c and Percp Cy5.5 anti-CD80 for 30 min at rt. After washing by PBS (×3), they were finally suspended in 0.5 mL of PBS and tested by flow cytometry.

TIL Analysis. Tumors were also cut into small pieces and digested in RPMI-1640 medium including 2% FCS, collagenase (50 U/mL), HAse (100 μg/mL), and DNase (50 U/mL) for 2 h at 37 °C. Then, the digested suspensions were filtrated, centrifuged, and washed with PBS (×3), then stained with Percp Cy5.5 CD3e and APC anti-CD8a for 30 min at rt. Following PBS washing three times, they were finally suspended in PBS (0.5 mL) and measured by flow cytometry.

Antitumor Efficacy and Abscopal Effect of CCPS/HPPH/DOX. All procedures were conducted in accordance with a protocol approved by the National Institutes of Health Clinical Center Animal Care and Use Committee (NIH CC/ACUC). For the antitumor efficacy study, we used MC38 colorectal carcinoma tumor bearing C57BL/6 mice (6–8 weeks) for primary and distant tumor therapeutics. First, 6×10^5 MC38 cells were subcutaneously inoculated in the right flank (primary tumor) and 2×10^5 cells were inoculated in the left side (distant tumor). On day 6 post-tumor inoculation, mice were randomly divided into five groups (n = 9/group) and injected with PBS, free DOX, CCPS/HPPH (+), CCPS/HPPH/DOX (−), and CCPS/HPPH/DOX (+) (DOX dose: 0.5 mg/kg, HPPH dose: 0.3 mg/kg) when primary tumors reached ∼100 mm^3. After 24 h, laser irradiation for right tumors was executed for mice treated with CCPS/HPPH (+) and CCPS/HPPH/DOX (+) at 671 nm (200 mW/cm^2, 10 min). The therapeutic process was merely a single injection, and from the treatment day, tumor volumes were measured by caliper every 3 days including left and right tumors and monitored within 18 days post-tumor inoculation. The volume formula is $V = (\text{length} \times \text{width}^2)/2$. The body weight was also recorded when tumor volumes were measured. The survival curves of mice in every group were also recorded.

Statistical Analysis. To compare differences between groups, one-way ANOVA with Tukey's multiple comparison tests were used. $^*p < 0.05$ was considered significant, and $^{**}p < 0.01$ and $^{***}p < 0.001$ were considered highly significant. Values were expressed as mean ± SD.

ASSOCIATED CONTENT

Supporting Information

The Supporting Information is available free of charge on the ACS Publications website at DOI: 10.1021/acsnano.8b08346.

Materials, characterization, synthesis of PEG-CPPA, synthesis of PEG-P(MMA-*co*-BAEMA), synthesis of PEG-P(MMA-*co*-AEMA(NH_2/SH)), drug loading test and *in vitro* drug release, cytotoxicity test of CCPS/HPPH/DOX, ICD induced by DOX and PDT from CPPS/HPPH/DOX for HMGB1 release, *in vivo* immune stimulation of CCPS/HPPH/DOX for cytokine test and DC maturation, $CD8^+$ T cells in spleen (PDF)

AUTHOR INFORMATION

Corresponding Authors

*E-mail: hushuo_xy@163.com.
*E-mail: shawn.chen@nih.gov.

ORCID

Zhen Yang: 0000-0003-4056-0347
Yunlu Dai: 0000-0003-4023-7320
Xiaoyuan Chen: 0000-0002-9622-0870

Notes

The authors declare no competing financial interest.

ACKNOWLEDGMENTS

This work was supported by the Intramural Research Program (IRP) of the National Institute of Biomedical Imaging and Bioengineering (NIBIB), National Institutes of Health (NIH), and National Natural Science Foundation of China (NSFC 81471689, 81771873, and 91859207). All animal experiments were performed under a National Institutes of Health Animal Care and Use Committee (NIH ACUC) approved protocol.

REFERENCES

(1) Melero, I.; Gaudernack, G.; Gerritsen, W.; Huber, C.; Parmiani, G.; Scholl, S.; Thatcher, N.; Wagstaff, J.; Zielinski, C.; Faulkner, I.; Mellstedt, H. Therapeutic Vaccines for Cancer: an Overview of Clinical Trials. *Nat. Rev. Clin. Oncol.* **2014**, *11*, 509–524.

(2) Hu, Z.; Ott, P. A.; Wu, C. J. Towards Personalized, Tumour-Specific, Therapeutic Vaccines for Cancer. *Nat. Rev. Immunol.* **2017**, *18*, 168–182.

(3) Byun, D. J.; Wolchok, J. D.; Rosenberg, L. M.; Girotra, M. Cancer Immunotherapy-Immune Checkpoint Blockade and Associated Endocrinopathies. *Nat. Rev. Endocrinol.* **2017**, *13*, 195–207.

(4) Mellman, I.; Coukos, G.; Dranoff, G. Cancer Immunotherapy Comes of Age. *Nature* **2011**, *480*, 480–489.

DOI: 10.1021/acsnano.8b08346
ACS Nano 2019, 13, 3083–3094

(5) Pardoll, D. M. The Blockade of Immune Checkpoints in Cancer Immunotherapy. *Nat. Rev. Cancer* **2012**, *12*, 252−264.
(6) Restifo, N. P.; Dudley, M. E.; Rosenberg, S. A. Adoptive Immunotherapy for Cancer: Harnessing the T Cell Response. *Nat. Rev. Immunol.* **2012**, *12*, 269−281.
(7) Rosenberg, S. A.; Restifo, N. P.; Yang, J. C.; Morgan, R. A.; Dudley, M. E. Adoptive Cell Transfer: a Clinical Path to Effective Cancer Immunotherapy. *Nat. Rev. Cancer* **2008**, *8*, 299−308.
(8) Palucka, K.; Banchereau, J. Cancer Immunotherapy *via* Dendritic Cells. *Nat. Rev. Cancer* **2012**, *12*, 265−277.
(9) Figdor, C. G.; de Vries, I. J.; Lesterhuis, W. J.; Melief, C. J. Dendritic Cell Immunotherapy: Mapping the Way. *Nat. Med.* **2004**, *10*, 475−480.
(10) Chen, H.; Zhang, W.; Zhu, G.; Xie, J.; Chen, X. Rethinking Cancer Nanotheranostics. *Nat. Rev. Mater.* **2017**, *2*, 17024.
(11) Cheung, A. S.; Mooney, D. J. Engineered Materials for Cancer Immunotherapy. *Nano Today* **2015**, *10*, 511−531.
(12) Fan, W.; Yung, B.; Huang, P.; Chen, X. Nanotechnology for Multimodal Synergistic Cancer Therapy. *Chem. Rev.* **2017**, *117*, 13566−13638.
(13) Irvine, D. J.; Hanson, M. C.; Rakhra, K.; Tokatlian, T. Synthetic Nanoparticles for Vaccines and Immunotherapy. *Chem. Rev.* **2015**, *115*, 11109−11146.
(14) Jo, S. D.; Nam, G.-H.; Kwak, G.; Yang, Y.; Kwon, I. C. Harnessing Designed Nanoparticles: Current Strategies and Future Perspectives in Cancer Immunotherapy. *Nano Today* **2017**, *17*, 23−37.
(15) Wang, C.; Sun, W.; Ye, Y.; Bomba, H. N.; Gu, Z. Bioengineering of Artificial Antigen Presenting Cells and Lymphoid Organs. *Theranostics* **2017**, *7*, 3504−3516.
(16) Weiden, J.; Tel, J.; Figdor, C. G. Synthetic Immune Niches for Cancer Immunotherapy. *Nat. Rev. Immunol.* **2017**, *18*, 212−219.
(17) Wang, C., Ye, Y., Hu, Q., Bellotti, A., Gu, Z. Tailoring Biomaterials for Cancer Immunotherapy: Emerging Trends and Future Outlook. *Adv. Mater.* **2017**, *29*, 1606036.
(18) Shi, J.; Kantoff, P. W.; Wooster, R.; Farokhzad, O. C. Cancer Nanomedicine: Progress, Challenges and Opportunities. *Nat. Rev. Cancer* **2017**, *17*, 20−37.
(19) von Roemeling, C.; Jiang, W.; Chan, C. K.; Weissman, I. L.; Kim, B. Y. S. Breaking Down the Barriers to Precision Cancer Nanomedicine. *Trends Biotechnol.* **2017**, *35*, 159−171.
(20) Chen, Q.; Xu, L.; Liang, C.; Wang, C.; Peng, R.; Liu, Z. Photothermal Therapy with Immune-Adjuvant Nanoparticles together with Checkpoint Blockade for Effective Cancer Immunotherapy. *Nat. Commun.* **2016**, *7*, 13193.
(21) Dai, L.; Li, K.; Li, M.; Zhao, X.; Luo, Z.; Lu, L.; Luo, Y.; Cai, K. Size/Charge Changeable Acidity-Responsive Micelleplex for Photodynamic-Improved PD-L1 Immunotherapy with Enhanced Tumor Penetration. *Adv. Funct. Mater.* **2018**, *28*, 1707249.
(22) Wang, D.; Wang, T.; Liu, J.; Yu, H.; Jiao, S.; Feng, B.; Zhou, F.; Fu, Y.; Yin, Q.; Zhang, P.; Zhang, Z.; Zhou, Z.; Li, Y. Acid-Activatable Versatile Micelleplexes for PD-L1 Blockade-Enhanced Cancer Photodynamic Immunotherapy. *Nano Lett.* **2016**, *16*, 5503−5513.
(23) Zhu, G.; Lynn, G. M.; Jacobson, O.; Chen, K.; Liu, Y.; Zhang, H.; Ma, Y.; Zhang, F.; Tian, R.; Ni, Q.; Cheng, S.; Wang, Z.; Lu, N.; Yung, B. C.; Wang, Z.; Lang, L.; Fu, X.; Jin, A.; Weiss, I. D.; Vishwasrao, H.; et al. Albumin/Vaccine Nanocomplexes that Assemble *in Vivo* for Combination Cancer Immunotherapy. *Nat. Commun.* **2017**, *8*, 1954.
(24) Peng, J.; Xiao, Y.; Li, W.; Yang, Q.; Tan, L.; Jia, Y.; Qu, Y.; Qian, Z. Photosensitizer Micelles Together with IDO Inhibitor Enhance Cancer Photothermal Therapy and Immunotherapy. *Adv. Sci.* **2018**, *5*, 1700891.
(25) Duan, X.; Chan, C.; Lin, W. Nanoparticle-Mediated Immunogenic Cell Death Enables and Potentiates Cancer Immunotherapy. *Angew. Chem., Int. Ed.* **2019**, *58*, 670−680.
(26) Galluzzi, L.; Buque, A.; Kepp, O.; Zitvogel, L.; Kroemer, G. Immunogenic Cell Death in Cancer and Infectious Disease. *Nat. Rev. Immunol.* **2017**, *17*, 97−111.
(27) Yang, Y.; Tang, J.; Abbaraju, P. L.; Jambhrunkar, M.; Song, H.; Zhang, M.; Lei, C.; Fu, J.; Gu, Z.; Liu, Y.; Yu, C. Hybrid Nanoreactors: Enabling an Off-the-Shelf Strategy for Concurrently Enhanced Chemo-Immunotherapy. *Angew. Chem., Int. Ed.* **2018**, *57*, 11764−11769.
(28) Fan, Y.; Kuai, R.; Xu, Y.; Ochyl, L. J.; Irvine, D. J.; Moon, J. J. Immunogenic Cell Death Amplified by Co-Localized Adjuvant Delivery for Cancer Immunotherapy. *Nano Lett.* **2017**, *17*, 7387−7393.
(29) He, C.; Duan, X.; Guo, N.; Chan, C.; Poon, C.; Weichselbaum, R. R.; Lin, W. Core-Shell Nanoscale Coordination Polymers Combine Chemotherapy and Photodynamic Therapy to Potentiate Checkpoint Blockade Cancer Immunotherapy. *Nat. Commun.* **2016**, *7*, 12499.
(30) Barker, H. E.; Paget, J. T.; Khan, A. A.; Harrington, K. J. The Tumour Microenvironment after Radiotherapy: Mechanisms of Resistance and Recurrence. *Nat. Rev. Cancer* **2015**, *15*, 409−425.
(31) Liu, Q.; Zhu, H.; Tiruthani, K.; Shen, L.; Chen, F.; Gao, K.; Zhang, X.; Hou, L.; Wang, D.; Liu, R.; Huang, L. Nanoparticle-Mediated Trapping of Wnt Family Member 5A in Tumor Microenvironments Enhances Immunotherapy for B-Raf Proto-Oncogene Mutant Melanoma. *ACS Nano* **2018**, *12*, 1250−1261.
(32) Mao, C.; Li, F.; Zhao, Y.; Debinski, W.; Ming, X. P-Glycoprotein-Targeted Photodynamic Therapy Boosts Cancer Nanomedicine by Priming Tumor Microenvironment. *Theranostics* **2018**, *8*, 6274−6290.
(33) Yu, X.; Gao, D.; Gao, L.; Lai, J.; Zhang, C.; Zhao, Y.; Zhong, L.; Jia, B.; Wang, F.; Chen, X.; Liu, Z. Inhibiting Metastasis and Preventing Tumor Relapse by Triggering Host Immunity with Tumor-Targeted Photodynamic Therapy Using Photosensitizer-Loaded Functional Nanographenes. *ACS Nano* **2017**, *11*, 10147−10158.
(34) Song, W.; Kuang, J.; Li, C. X.; Zhang, M.; Zheng, D.; Zeng, X.; Liu, C.; Zhang, X. Z. Enhanced Immunotherapy Based on Photodynamic Therapy for Both Primary and Lung Metastasis Tumor Eradication. *ACS Nano* **2018**, *12*, 1978−1989.
(35) Yang, G.; Xu, L.; Xu, J.; Zhang, R.; Song, G.; Chao, Y.; Feng, L.; Han, F.; Dong, Z.; Li, B.; Liu, Z. Smart Nanoreactors for pH-Responsive Tumor Homing, Mitochondria-Targeting, and Enhanced Photodynamic-Immunotherapy of Cancer. *Nano Lett.* **2018**, *18*, 2475−2484.
(36) Lovell, J. F.; Liu, T. W. B.; Chen, J.; Zheng, G. Activatable Photosensitizers for Imaging and Therapy. *Chem. Rev.* **2010**, *110*, 2839−2857.
(37) Li, A. W.; Sobral, M. C.; Badrinath, S.; Choi, Y.; Graveline, A.; Stafford, A. G.; Weaver, J. C.; Dellacherie, M. O.; Shih, T. Y.; Ali, O. A.; Kim, J.; Wucherpfennig, K. W.; Mooney, D. J. A Facile Approach to Enhance Antigen Response for Personalized Cancer Vaccination. *Nat. Mater.* **2018**, *17*, 528−534.
(38) Luo, M.; Wang, H.; Wang, Z.; Cai, H.; Lu, Z.; Li, Y.; Du, M.; Huang, G.; Wang, C.; Chen, X.; Porembka, M. R.; Lea, J.; Frankel, A. E.; Fu, Y. X.; Chen, Z. J.; Gao, J. A STING-Activating Nanovaccine for Cancer Immunotherapy. *Nat. Nanotechnol.* **2017**, *12*, 648−654.
(39) He, Y.; Hara, H.; Nunez, G. Mechanism and Regulation of NLRP3 Inflammasome Activation. *Trends Biochem. Sci.* **2016**, *41*, 1012−1021.
(40) Liu, Q.; Jia, J.; Yang, T.; Fan, Q.; Wang, L.; Ma, G. Pathogen-Mimicking Polymeric Nanoparticles based on Dopamine Polymerization as Vaccines Adjuvants Induce Robust Humoral and Cellular Immune Responses. *Small* **2016**, *12*, 1744−1757.
(41) Nochi, T.; Yuki, Y.; Takahashi, H.; Sawada, S.; Mejima, M.; Kohda, T.; Harada, N.; Kong, I. G.; Sato, A.; Kataoka, N.; Tokuhara, D.; Kurokawa, S.; Takahashi, Y.; Tsukada, H.; Kozaki, S.; Akiyoshi, K.; Kiyono, H. Nanogel Antigenic Protein-Delivery System for Adjuvant-Free Intranasal Vaccines. *Nat. Mater.* **2010**, *9*, 572−578.
(42) Chu, J.; Thomas, L. M.; Watkins, S. C.; Franchi, L.; Nunez, G.; Salter, R. D. Cholesterol-Dependent Cytolysins Induce Rapid Release of Mature IL-1β from Murine Macrophages in a NLRP3 Inflammasome and Cathepsin B-Dependent Manner. *J. Leukocyte Biol.* **2009**, *86*, 1227−1238.
(43) Deng, Z.; Qian, Y.; Yu, Y.; Liu, G.; Hu, J.; Zhang, G.; Liu, S. Engineering Intracellular Delivery Nanocarriers and Nanoreactors from Oxidation-Responsive Polymersomes *via* Synchronized Bilayer Cross-Linking and Permeabilizing Inside Live Cells. *J. Am. Chem. Soc.* **2016**, *138*, 10452−10466.

DOI: 10.1021/acsnano.8b08346
ACS Nano 2019, 13, 3083−3094

(44) Yang, W.; Xia, Y.; Zou, Y.; Meng, F.; Zhang, J.; Zhong, Z. Bioresponsive Chimaeric Nanopolymersomes Enable Targeted and Efficacious Protein Therapy for Human Lung Cancers *In Vivo*. *Chem. Mater.* **2017**, *29*, 8757−8765.
(45) Molla, M. R.; Rangadurai, P.; Antony, L.; Swaminathan, S.; de Pablo, J. J.; Thayumanavan, S. Dynamic Actuation of Glassy Polymersomes through Isomerization of a Single Azobenzene Unit at The Block Copolymer Interface. *Nat. Chem.* **2018**, *10*, 659−666.
(46) Li, Y.; Liu, G.; Wang, X.; Hu, J.; Liu, S. Enzyme-Responsive Polymeric Vesicles for Bacterial-Strain-Selective Delivery of Antimicrobial Agents. *Angew. Chem., Int. Ed.* **2016**, *55*, 1760−1764.
(47) Rideau, E.; Dimova, R.; Schwille, P.; Wurm, F. R.; Landfester, K. Liposomes and Polymersomes: a Comparative Review towards Cell Mimicking. *Chem. Soc. Rev.* **2018**, *47*, 8572−8610.
(48) Wang, X.; Liu, G.; Hu, J.; Zhang, G.; Liu, S. Concurrent Block Copolymer Polymersome Stabilization and Bilayer Permeabilization by Stimuli-Regulated "Traceless" Crosslinking. *Angew. Chem., Int. Ed.* **2014**, *53*, 3138−3142.
(49) Che, H.; Cao, S.; van Hest, J. C. M. Feedback-Induced Temporal Control of "Breathing" Polymersomes to Create Self-Adaptive Nanoreactors. *J. Am. Chem. Soc.* **2018**, *140*, 5356−5359.
(50) Hu, X.; Zhai, S.; Liu, G.; Xing, D.; Liang, H.; Liu, S. Concurrent Drug Unplugging and Permeabilization of Polyprodrug-Gated Cross-linked Vesicles for Cancer Combination Chemotherapy. *Adv. Mater.* **2018**, *30*, 1706307.
(51) Yang, W.; Zou, Y.; Meng, F.; Zhang, J.; Cheng, R.; Deng, C.; Zhong, Z. Efficient and Targeted Suppression of Human Lung Tumor Xenografts in Mice with Methotrexate Sodium Encapsulated in All-Function-in-One Chimeric Polymersomes. *Adv. Mater.* **2016**, *28*, 8234−8239.
(52) Li, Y.; Xiao, K.; Zhu, W.; Deng, W.; Lam, K. S. Stimuli-Responsive Cross-Linked Micelles for on-Demand Drug Delivery against Cancers. *Adv. Drug Delivery Rev.* **2014**, *66*, 58−73.
(53) Cheng, R.; Meng, F.; Deng, C.; Klok, H.-A.; Zhong, Z. Dual and Multi-Stimuli Responsive Polymeric Nanoparticles for Programmed Site-Specific Drug Delivery. *Biomaterials* **2013**, *34*, 3647−3657.
(54) Pikabea, A.; Forcada, J. Novel Approaches for The Preparation of Magnetic Nanogels *via* Covalent Bonding. *J. Polym. Sci., Part A: Polym. Chem.* **2017**, *55*, 3573−3586.
(55) Lee, A. S.; Inayathullah, M.; Lijkwan, M. A.; Zhao, X.; Sun, W.; Park, S.; Hong, W. X.; Parekh, M. B.; Malkovskiy, A. V.; Lau, E. Prolonged Survival of Transplanted Stem Cells after Ischaemic Injury *via* the Slow Release of Pro-Survival Peptides from A Collagen Matrix. *Nat. Biomed. Eng.* **2018**, *2*, 104.
(56) He, H.; Cattran, A. W.; Nguyen, T.; Nieminen, A. L.; Xu, P. Triple-Responsive Expansile Nanogel for Tumor and Mitochondria Targeted Photosensitizer Delivery. *Biomaterials* **2014**, *35*, 9546−9553.
(57) Lyu, Y. L.; Kerrigan, J. E.; Lin, C. P.; Azarova, A. M.; Tsai, Y. C.; Ban, Y.; Liu, L. F. Topoisomerase IIbeta Mediated DNA Double-Strand Breaks: Implications in Doxorubicin Cardiotoxicity and Prevention by Dexrazoxane. *Cancer Res.* **2007**, *67*, 8839−8846.
(58) Fan, W.; Lu, N.; Xu, C.; Liu, Y.; Lin, J.; Wang, S.; Shen, Z.; Yang, Z.; Qu, J.; Wang, T.; Chen, S.; Huang, P.; Chen, X. Enhanced Afterglow Performance of Persistent Luminescence Implants for Efficient Repeatable Photodynamic Therapy. *ACS Nano* **2017**, *11*, 5864−5872.
(59) Wang, S.; Yu, G.; Wang, Z.; Jacobson, O.; Tian, R.; Lin, L. S.; Zhang, F.; Wang, J.; Chen, X. Hierarchical Tumor Microenvironment-Responsive Nanomedicine for Programmed Delivery of Chemotherapeutics. *Adv. Mater.* **2018**, *30*, 1803926.

DOI: 10.1021/acsnano.8b08346
ACS Nano 2019, 13, 3083−3094